Additive Manufacturing Letters 1 (2021) 100003

Contents lists available at ScienceDirect

Additive Manufacturing Letters

journal homepage: www.elsevier.com/locate/addlet

In-situ synchrotron X-ray diffraction analysis of the elastic behaviour of martensite and H-phase in a NiTiHf high temperature shape memory alloy fabricated by laser powder bed fusion

Jiajia Shen[a], Zhi Zeng[b], Mohammadreza Nematollahi[c], Norbert Schell[d], Emad Maawad[d], R.N. Vasin[e], Keyvan Safaei[c], Behrang Poorganji[c], Mohammad Elahinia[c], J.P. Oliveira[a,*]

[a] UNIDEMI, Department of Mechanical and Industrial Engineering, NOVA School of Science and Technology, Universidade NOVA de Lisboa, 2829-516 Caparica, Portugal
[b] School of Mechanical and Electronic Engineering, University of Electronic Science and Technology of China, Chengdu, Sichuan 611731, China
[c] Dynamic and Smart Systems Laboratory, MIME Department, University of Toledo, Toledo, OH 43606, USA
[d] Institute of Materials Physics, Helmholtz-Zentrum Hereon, Max-Planck-Str. 1, D-21502 Geesthacht, Germany
[e] Frank Laboratory of Neutron Physics, Joint Institute for Nuclear Research, 141980 Dubna, Russia

ARTICLE INFO

Keywords:
NiTiHf shape memory alloys
synchrotron radiation
martensite
H-phase
laser powder bed fusion
additive manufacturing

ABSTRACT

High temperature shape memory alloys of the Ni-Ti-Hf system are potential candidates for aerospace applications where powder bed additive manufacturing technologies are being increasingly used. In this work, a Ti-rich NiTiHf high temperature shape memory alloy powder was processed by laser powder bed fusion. The standard heat treatment of 550 ^{0}C for 3 hours was imposed to promote H-phase precipitation. At room temperature, the material has a dual-phase microstructure composed of martensite, the matrix, and H-phase, as a strengthening precipitate. High energy synchrotron X-ray diffraction is used to evaluate, in-situ, the elastic behaviour of the fabricated part. The deformation anisotropy of several (h k l) families of planes of both phases is evidenced. No major texture changes were observed upon macroscopic elastic loading. We illustrate the potential of using high energy synchrotron X-ray diffraction for detailed analyses of minority phases in additively manufactured components.

Introduction

The poor machinability of NiTi-based shape memory alloys usually requires advanced manufacturing techniques to create complex shaped geometries. Among the available technologies for such, fusion-based processes, namely welding and additive manufacturing, are widely used [1,2]. Although additive manufacturing of shape memory alloys is primarily devoted to (near)equiatomic NiTi [3–5], recent works have shown the viability to obtain parts based on the Ni-Ti-Hf system [6]. Among the several additive manufacturing technologies available for processing metallic materials, laser powder bed fusion is the most employed. Here, three-dimensional structures can be fabricated in a layer-by-layer fashion using a laser as the heat source. Given the reduced dimension of the heat source, laser powder bed fusion additive manufacturing is known for its high geometrical accuracy, suitable to fabricate components with higher feature resolution, and tighter dimensional accuracy for multiple industries including, but not limited, to biomedical and aerospace.

High temperature shape memory alloys based on the Ni-Ti-X systems (with X potentially being Hf, Zr, or Au, among others) are potential candidates for advanced engineering applications, especially in the aerospace field, as in shape morphing structures. These alloys, unlike conventional (near)equiatomic NiTi alloys, show transformation temperatures well above 100 ºC. Ni-Ti-X alloys with X = Hf are currently the most used high temperature alloys given their superior mechanical properties and stability when appropriate thermomechanical processing is employed. Despite the unique capabilities of NiTiHf alloys, the weak machinability of these materials, similar to NiTi, is the major roadblock to developing components with complex shapes. Recently, motivated by the issue associated with machinability, the authors have conducted research on developing the laser powder bed fusion technique for processing high temperature NiTiHf shape memory alloys [7].

The thermomechanical behaviour of NiTi-based shape memory alloys is greatly dependent on its microstructure characteristics, i.e., their stable phases and volume fraction, which arise from thermomechanical processing. Three major phases are typically reported for NiTiHf high-

* Corresponding author.
E-mail address: jp.oliveira@fct.unl.pt (J.P. Oliveira).

https://doi.org/10.1016/j.addlet.2021.100003
Received 29 May 2021; Received in revised form 24 June 2021; Accepted 28 June 2021
2772-3690/© 2021 The Author(s). Published by Elsevier B.V. This is an open access article under the CC BY-NC-ND license (http://creativecommons.org/licenses/by-nc-nd/4.0/)

temperature shape memory alloys: B2 austenite (BCC), B19' martensite (monoclinic), and orthorhombic H-phase. While B2 and B19' phases are intrinsic to NiTi-based shape memory alloys, as their high and low-temperature phases, respectively, H-phase acts as a strengthening precipitate for NiTiHf (and NiTiZr) alloys and is developed as the result of proper heat treatments. In other words, H-phase precipitation is an desirable phase to increase the thermal stability and shape memory recovery [8]. The most used heat treatment process for NiTiHf (or NiTiZr) high temperature shape memory alloys consists of a 3-hour heating at 550 ºC followed by an air cooling, which generates fine, nanometric, plate-like H-phase precipitates [9–11]. Although, using neutrons and synchrotron X-ray diffraction, the in-situ mechanical behaviour of B2 austenite and B19' martensite have been previously studied [12–16], the behaviour of H-phase requires additional research. Prior in-situ studies have shown that during thermomechanical loading, the austenite phase tends to deform in an isotropic way, whereas the monoclinic B19' is highly anisotropic. This can be related to the crystal structures of each phase: austenite has a body-centred cubic structure, while martensite has a low symmetry monoclinic crystal structure [13].

So far, very little is known about the in-situ mechanical response during thermomechanical loading of H-phase. Several constraints exist that may justify the little knowledge on this topic. In-situ deformation techniques to probe the deformation response of distinct phases primarily consist of diffraction-based methods. However, the typical volume fraction of the H-phase after optimum heat treatment conditions is around 7 to 8 % [17]. The low volume fraction of this phase renders low-intensity peaks in those diffraction-based techniques. Moreover, when tested below the stability domain of austenite, the presence of the low symmetry B19' phase translates into multiple and broad diffraction peaks that often hinder those corresponding to H-phase. In addition, when using conventional laboratorial X-ray sources, the background noise of the measurement impacts the clear observation of these low-intensity peaks. One way to overcome these challenges is using high-energy synchrotron X-ray diffraction. The high signal-to-noise ratio allows to clearly identify minor phases, which coupled to the high photon flux and high energy, enables performing measurements with very small (dozens of microns or less) beam sizes in short periods of time (few seconds or less per analysed spot, depending on the material and its thickness). Another important feature associated with transmission-based synchrotron X-ray diffraction is the ability to characterise the microstructure evolution as a function of the orientation of the sample to the photon beam and detector plane. Implementing this technique during in-situ analysis allows to probe the evolution of different phases when a given thermomechanical condition is imposed.

In this work, the elastic deformation of a Ti-rich NiTiHf high temperature shape memory alloy fabricated by laser powder bed fusion and post-processed by heat-treatment to promote the precipitation of H-phase is studied in-situ using high energy synchrotron X-ray diffraction. The anisotropic deformation of both martensite and H-phase is determined and discussed.

Experimental procedure

The $Ni_{49.8}Ti_{30.2}Hf_{20}$ (at. %) high temperature shape memory alloy was fabricated by laser powder bed fusion additive manufacturing as described previously [6]. Samples for in-situ compression tests were fabricated with a diameter of 3 mm and a height of 5 mm. To remove the surface roughness of the as-built samples, fine sandpaper was used to smooth the material surface. The as-built samples are fully martensitic at room temperature with no traces of H-phase precipitates given the relatively low transformation kinetics associated with this phase. To promote H-phase precipitation, the as-built samples were consecutively heat treated at 950 and 550 ºC for 3 hours at each temperature. The first heat treatment (950 ºC / 3 hours) aims to erase the non-equilibrium solidification microstructure of the fabricated parts, which inhibits the homogenous formation of H-phase. The second heat treatment at 550 ºC

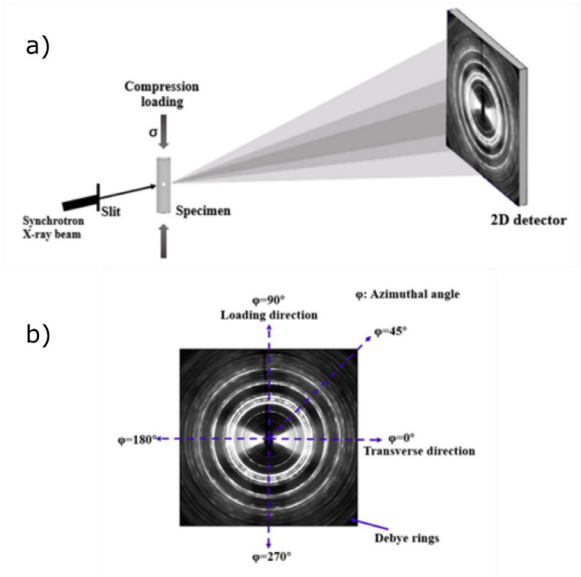

Fig. 1. a) Setup used for the in-situ X-ray diffraction measurements during macroscopic elastic loading; b) Debbye-Scherrer diffraction rings and definition of the azimuthal angles in the laboratorial reference frame.

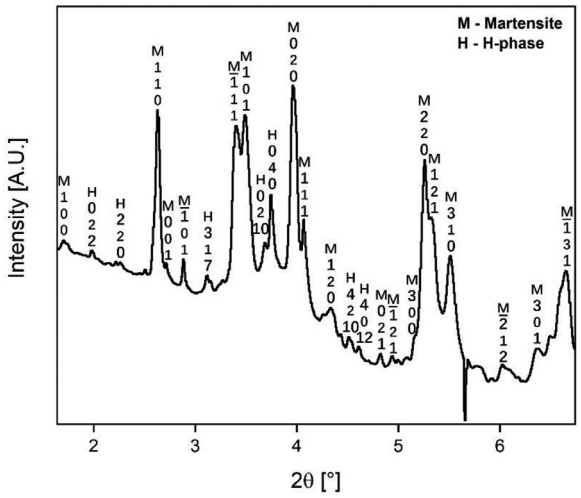

Fig. 2. X-ray diffraction pattern of the NiTiHf sample after double step heat treatment of 950ºC/3hour + 550ºC/3hour.

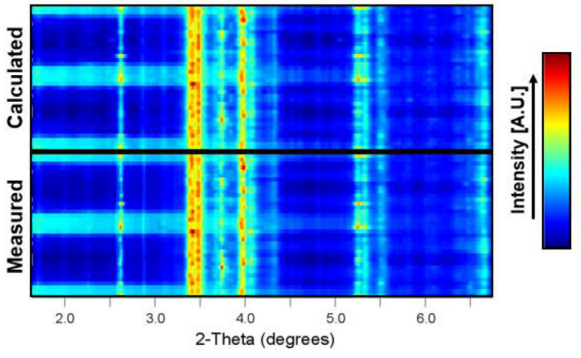

Fig. 3. 2D Rietveld refinement plot prior to any imposed load.

Table 1
Correspondence between the 2D images captured during in-situ mechanical testing and the corresponding macroscopic stress/strain values.

Image #	Stress [MPa]	Strain [%]
1	0	0
2	100	1
3	220	2

for 3 hours targets the H-phase precipitation, which is known to improve the mechanical stability of these alloys [18].

Synchrotron X-ray diffraction experiments were performed at the P07B High Energy Materials Science beamline of the Helmholtz-Zentrum Hereon at DESY. A 2D Perkin Elmer fast detector was used. Calibration of the experimental setup (sample-to-detector distance) and instrumental resolution function due to the optical and instrumental layout of the beamline was performed using standard LaB_6 powder. The wavelength used for these experiments was 0.14235 Å, while the calibrated sample-to-detector distance was of 1396 mm. The setup used for the synchrotron X-ray diffraction measurements is schematically shown in Figure 1 a. Due to the large absorptivity of the alloy induced by the significant presence of Hf, the exposure time for each 2D image was of 20 seconds, which is still significantly lower than when using neutron sources. In-situ compression testing, within the elastic behaviour region was performed at room temperature. Three 2D images were taken at different stress/strain levels as detailed in Table 1. After the acquisition of the 2D images, the raw data was treated using a combination of Fit2D [19,20], GSAS-II [21], Jade9 and MAUD [22].

The lattice strain (in units of microstrain) for selected (h k l) planes, ε_{hkl}, was determined using Equation (1):

$$\varepsilon_{hkl} = \frac{d_x - d_0}{d_0}\left(x10^6\right) \quad (1)$$

where d_x corresponds to the d-spacing of a specific (h k l) family at a given stress/strain level and d_0 corresponds to the d-spacing of the same (h k l) family in the stress-free condition. For reference, the lattice strain before loading is assumed to be 0, since $d_x = d_0$ in this case.

The macroscopic compressive load was applied normal to the incident X-ray beam (refer to Figure 1 a). Therefore, induced anisotropic elastic deformation in the sample is manifested as distortion of the Debye-Scherrer rings into ellipses. Therefore, to observe the directional strain anisotropy, lattice strains during macroscopic elastic loading for selected (h k l) family planes of martensite and H-phase were calculated from different diffraction patterns obtained by integration of the diffraction image in 10º azimuthal steps.

Considering the laboratory reference (refer to Fig. 1 b), the φ = 90 and 270º azimuthal angles are aligned with the compression direction, whereas the φ = 0 and 180º azimuthal angles are perpendicular to the loading direction.

Results and discussion

Starting microstructure

Previous characterization of the microstructure of the material used in this work has been performed by the authors in [6,23], thus we refrain to discuss it here and attention is paid to the unique in-situ X-ray diffraction measurements performed.

The X-ray diffraction pattern after full azimuthal integration of the virgin heat-treated NiTiHf sample is depicted in Fig. 2. Martensite and H-phase are indexed in the diffraction pattern and no evidence of austenite is observed. Hf-based oxides can be assigned to the non-indexed diffraction peaks and these occur owing to the extremely high affinity of Hf with oxygen during laser processing [18]. Rietveld refinement was performed (refer to Fig. 3) to determine the volume fractions of martensite and H-phase that are 92 and 8 %, respectively. The volume fractions obtained in this work are in good agreement with other studies on high-temperature shape memory alloys where the 550 ºC / 3-hour heat treatment was used to promote H-phase precipitation [17]. For reference, the stress-free lattice parameters of both martensite and H-phase determined by Rietveld refinement are reported in Table 2.

Table 2
Lattice parameters of martensite and H-phase before mechanical loading.

Phase	a [nm]	b [nm]	c [nm]	α [^{0}]	β [^{0}]	γ [^{0}]
Martensite	4.9061	4.0913	3.0648	90	103.718	90
H-phase	12.449	8.7145	25.806	90	90	90

Phase- and crystal orientation-dependent mechanical behaviour

In this work, four martensite and two H-phase diffraction peaks were selected to evaluate the lattice strain evolution as a function of the applied stress. The selected (h k l) planes for martensite are (1 0 0), (-1 0 1), (0 2 0) and (1 1 1), while the (0 2 10) and (0 4 0) planes are the selected ones for H-phase. The reason for this selection is related to the fact that these peaks are either isolated and/or have high intensity for most azimuthal angles, which prevents any misidentification upon the use of the peak fitting procedure.

The lattice strain evolution as a function of the azimuthal angle and imposed stress for the selected martensite and H-phase diffraction peaks is shown in Fig. 4. For the sake of comparison, the polar plots in Fig. 4 have the same scale. As it will be shown and discussed later, the mechanical responses do not show similar behaviour for different families of planes of both martensite and H-phase in the elastic region. For that reason, Figs. 5 and 6 illustrate similar polar plots focusing only on the analysed (h k l) planes of martensite and H-phase, respectively.

Considering the analysed martensite diffraction planes, all peaks show a similar behaviour except for the (-1 0 1) plane. Upon the compressive loading, a negative strain is generated along the loading direction (corresponding to the azimuthal angles of 90 and 270 º), whereas in the traverse direction (at 0 and 180 º) a positive strain develops due to the Poisson effect. This phenomenon was also observed in other studies analysing the mechanical behaviour of the low-temperature martensitic phase during in-situ measurements on NiTi shape memory alloys [24]. For the (-1 0 1) martensite peak (refer to Figs. 4 b and 5) a completely distinct behaviour occurs in a way that a positive (tensile) strain is preferentially developed along the 90 to 270 º azimuthal angles, while a negative (compressive) strain forms in the remaining two quadrants. This is most likely related to the orientation-dependency that arises from the texture inherited from the parent austenite phase that determines the deformation behaviour of martensite in shape memory alloys [25].

The most striking observation is the high anisotropy in the mechanical response of both martensite and H-phase upon loading within the elastic region. For martensite, this can be linked to the low symmetry of the monoclinic phase [13]. As for the orthorhombic H-phase, this is related to the preferential orientation at which H-phase precipitates form in the parent (austenite) phase. Moreover, the existence of a composite-like structure composed of martensite and H-phase may require the deformation of both phases in an anisotropic way to accommodate: i) their lattice mismatch [26]; ii) their different mechanical response under a given external load as a result of their distinct mechanical behaviour.

Previous work by Benafan et al. [13] showed that for a similar NiTiHf high temperature shape memory alloy tested within the macroscopic elastic domain, the B2 cubic austenite showed no evidence of anisotropic behaviour for any specific (azimuthal) direction. As for martensite, the

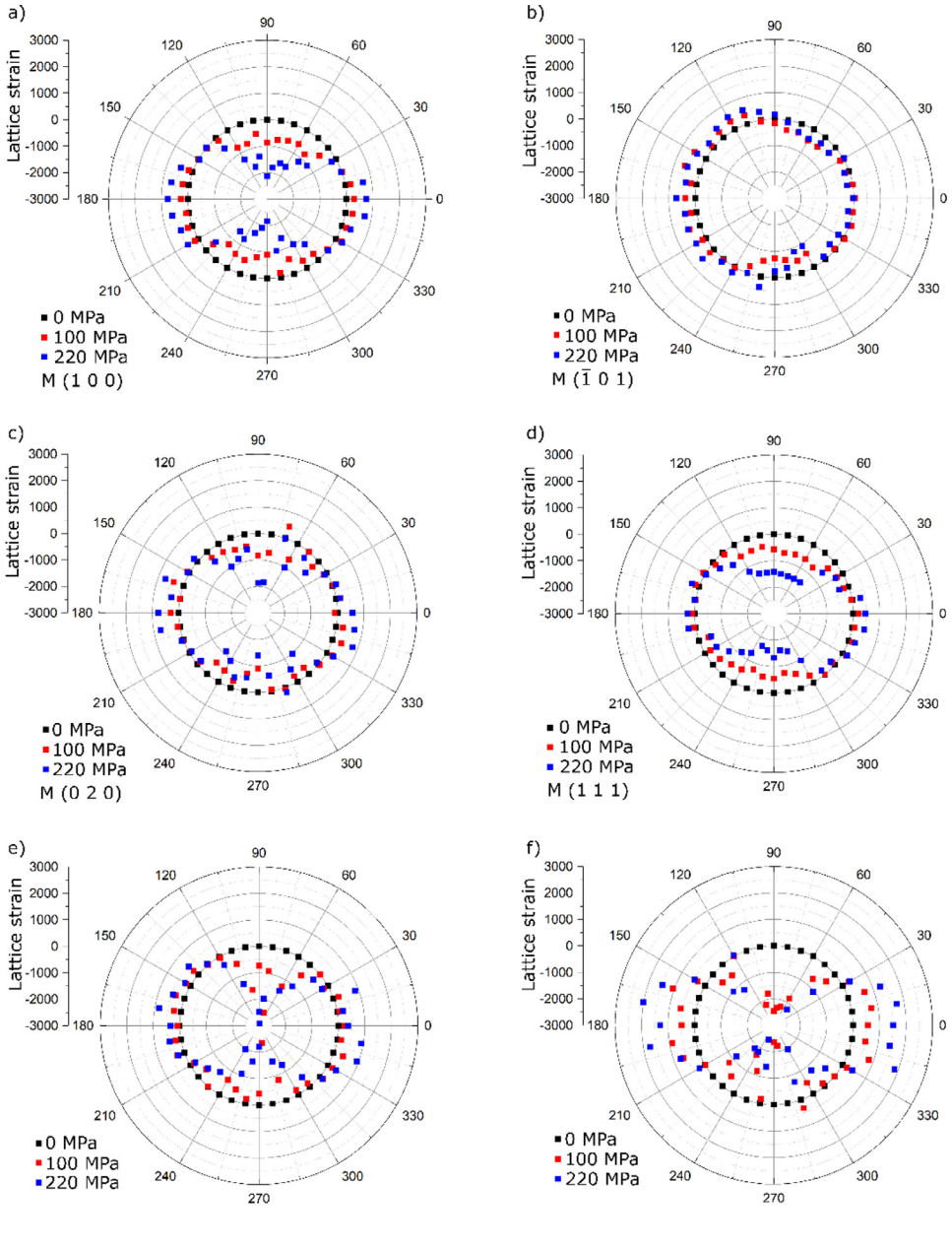

Fig. 4. Polar plots relating the lattice strain evolution over the azimuthal angle for the (1 0 0), (-1 0 1), (0 2 0) and (1 1 1), martensite peaks as well as (0 2 10) and (0 4 0) H-phase planes, for externally applied compression stresses of 0, 100 and 220 MPa. The stress-free condition (0 MPa) corresponds to the d-spacing reference from which the lattice strain was calculated. Note that for the H-phase (0 4 0) plane, the lattice strain range (set from -3000 to 3000 here) falls outside the minimum lattice strain obtained along the compression direction (≈- 5500). A complete view of the lattice strain evolution as a function of the azimuthal angle for this plane is further detailed in Fig. 6 b).

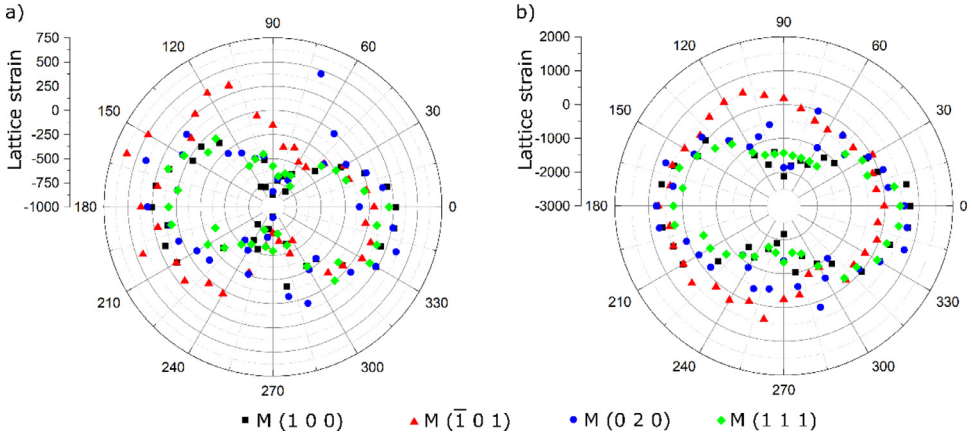

Fig. 5. Polar plots relating the lattice strain evolution dependence with the azimuthal angle for (1 0 0), (-1 0 1), (0 2 0) and (1 1 1) martensite peaks for applied compression stresses of: a) 100 MPa; b) 200 MPa.

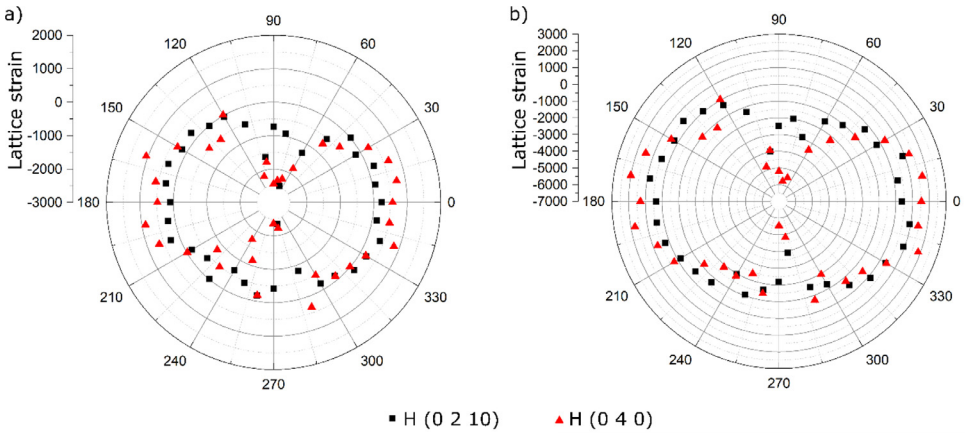

Fig. 6. Polar plots relating the lattice strain evolution dependence with the azimuthal angle for (0 2 10) and (0 4 0) H-phase peaks for applied compression stresses of: a) 100 MPa; b) 200 MPa.

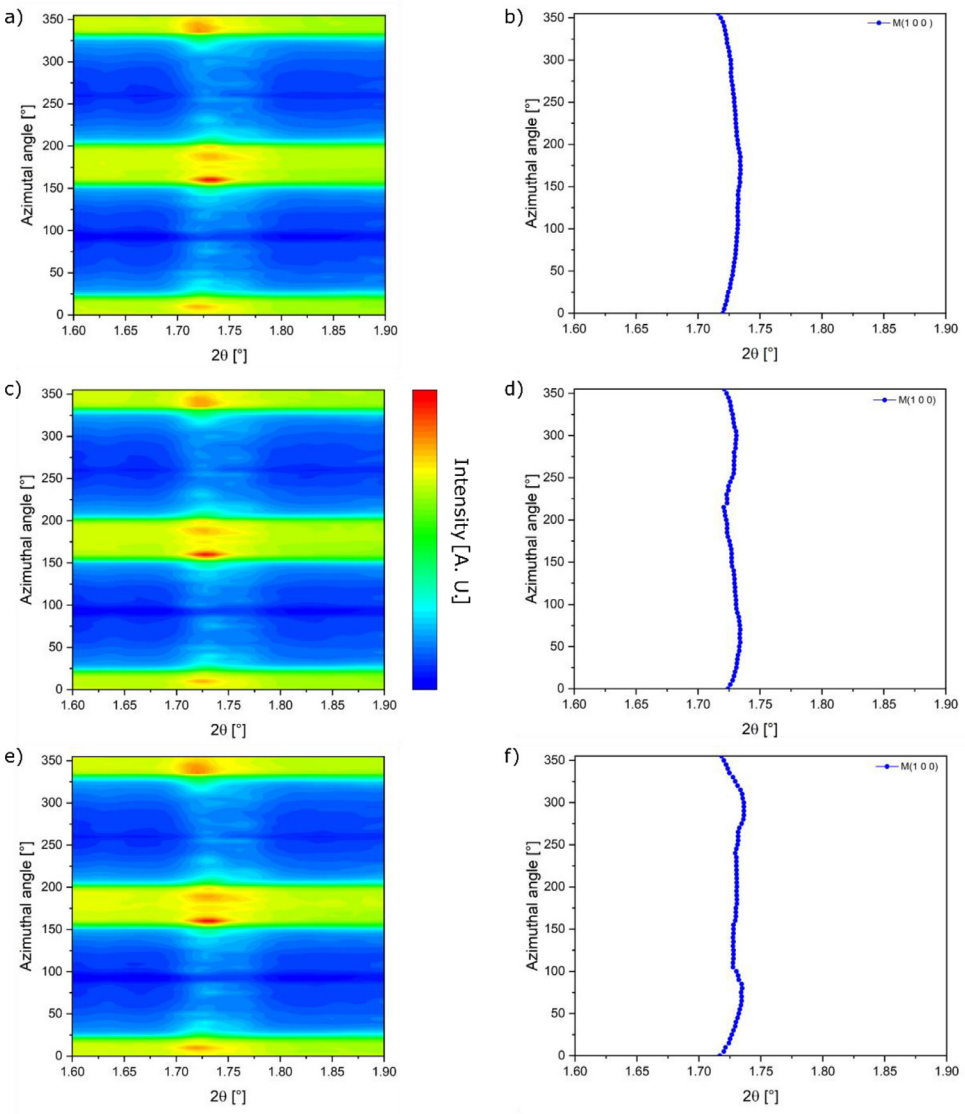

Fig. 7. Contour plot detailing the evolution of the diffracted intensity of martensite peak M (1 0 0) as a function of the azimuthal and diffraction angle under different loading conditions: a and b) before loading; c and d) 100MPa; e and f) 220MPa.

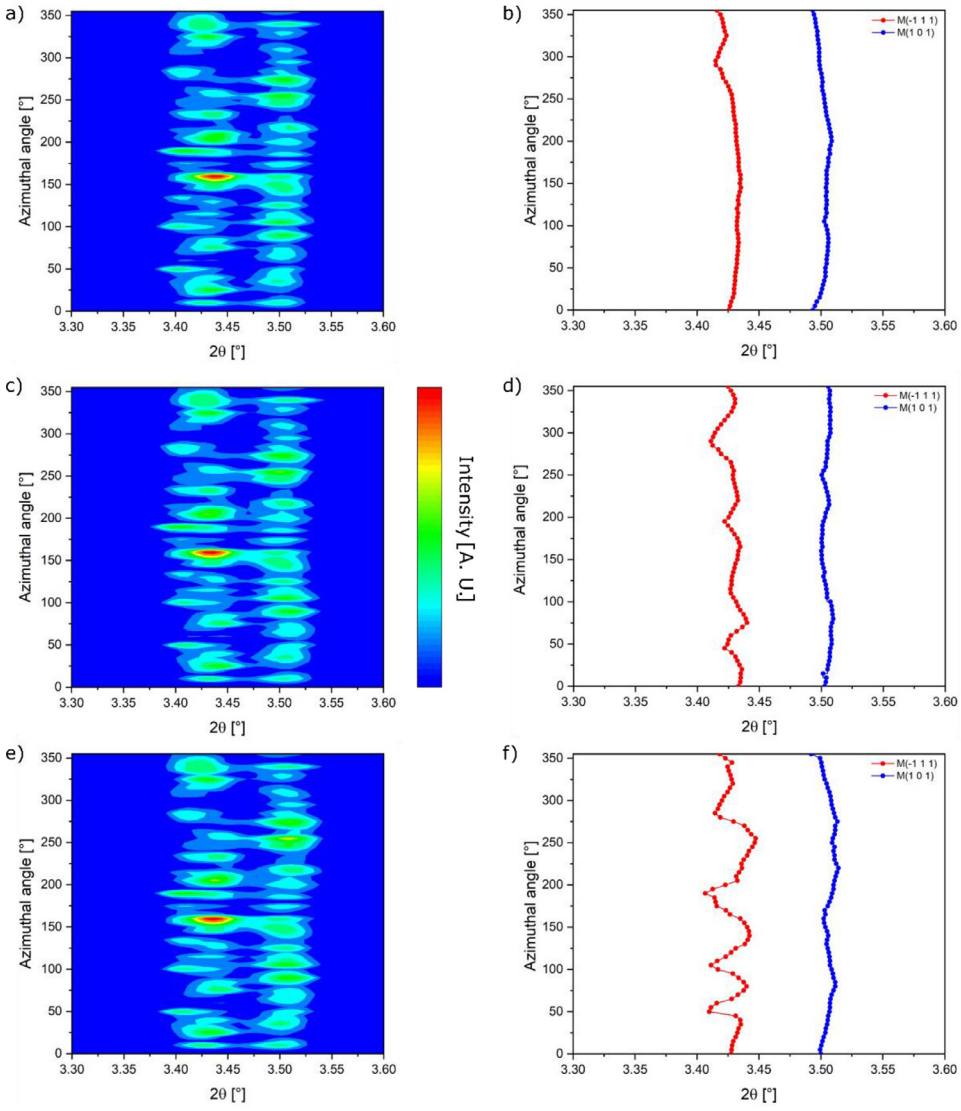

Fig. 8. Contour plot detailing the evolution of the diffracted intensity of martensite peaks M (-1 1 1) and M (1 0 1) as a function of the azimuthal and diffraction angle under different loading conditions: a and b) before loading; c and d) 100MPa; e and f) 200MPa.

work of Benafan et al. [13] reported an anisotropic behaviour similar to the present study. Though both works have used almost similar loading scenarios (100 and 220 MPa here and 100, 200, and 300 MPa in [13], the anisotropy in martensite is more significant in the present work compared to Benafan's et al. work. This can be attributed to the different manufacturing processes used to obtain the materials in both works. In [13], extruded rods with a 550 ºC/3-hour heat-treatment for H-phase precipitation were used, while here the material was processed by laser powder bed fusion technique followed by a 950 ºC/3-hour + 550 ºC/3-hour heat-treatment schedule. As a result, some typical microstructure features from both manufacturing routes can slightly modify the micromechanical response of the existing phases. In particular, the extruded and heat-treated rods had an average grain size of approximately 25 μm, which is lower than the average grain size of ≈ 50 μm in the present additively manufactured samples [6]. Moreover, texture effects arising from the additive manufacturing process can also play a role in its micromechanical behaviour. In fact, during laser powder bed fusion, a highly textured microstructure is developed because of the steep solidification conditions. Though a two-step heat treatment was imposed to reset the material's microstructure, it is possible that some remaining texture induced by the laser powder bed fusion process still influences the mechanical response of the alloy.

Further qualitative assessment of the evolution of the material texture during macroscopic elastic loading is further evidenced in the contour plots of Figs. 7–10 (a, c, and e). Here, for each analysed loading condition (0, 100, and 220 MPa) the peak intensity and corresponding diffraction angle of selected (h k l) planes are detailed in cartesian coordinates to better illustrate the dependence of the peak position (shifts in the diffraction angle) over the azimuthal angle. To further evidence these changes, especially for low-intensity diffraction peaks, each of the contour plots is combined with the actual position of the corresponding diffraction peak along the azimuthal angle (refer to Figs. 7–10 b, d and f). Indeed, changes of diffraction peak intensities with the azimuthal angle φ indicate the presence of preferred orientation. There are no changes with increasing macroscopic stress, which confirms purely elastic deformation mode. It is further observed (see for example Figs. 8 and 10 a) that some high intensity regions are located at apparently random azimuthal angles. This is related to the relatively large grain size of the analysed sample: when this/these grain/s is/are in diffraction condition for a certain azimuthal angle a very high intensity is captured. The evo-

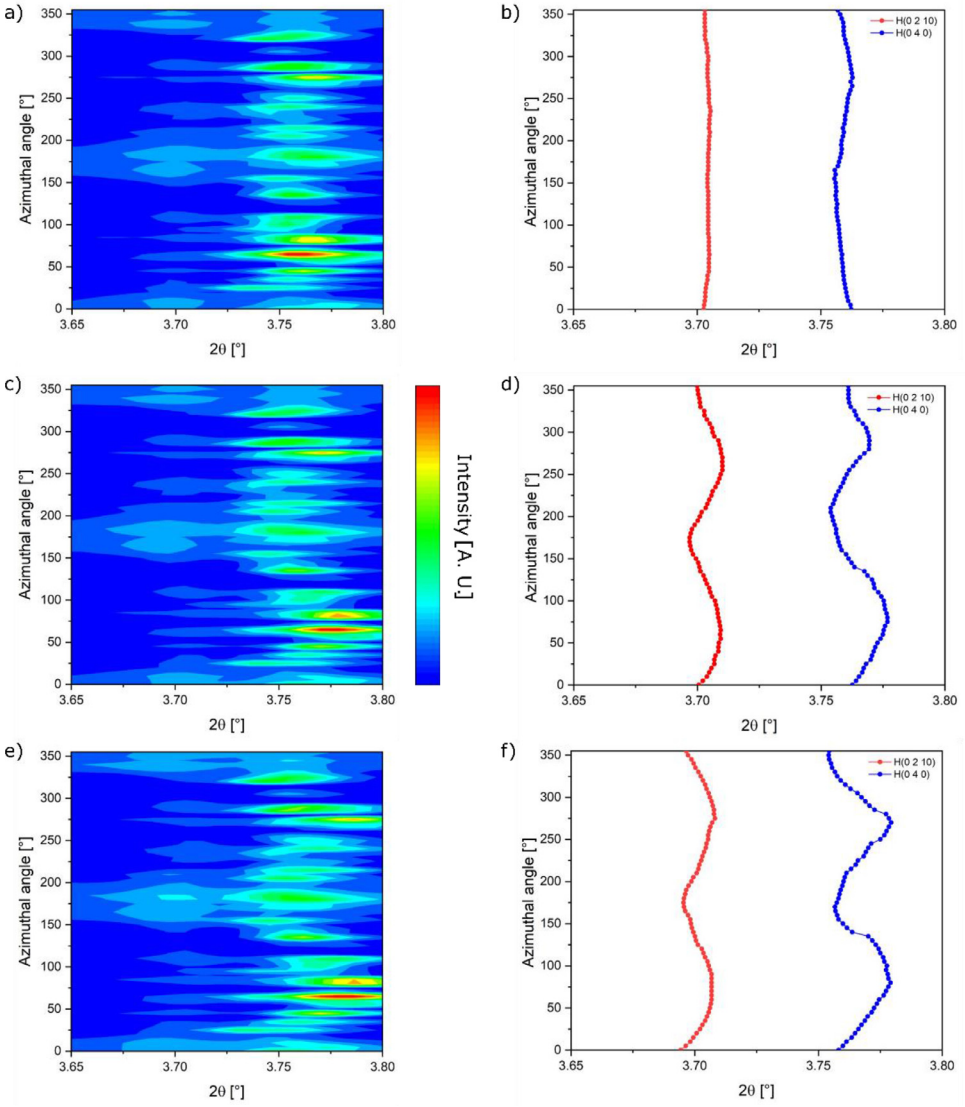

Fig. 9. Contour plot detailing the evolution of the diffracted intensity of H-phase peaks H (0 2 10) and H (0 4 0) as a function of the azimuthal and diffraction angle under different loading conditions: a and b) before loading; c and d) 100 MPa; e and f) 220 MPa.

lution of the peak positions detailed in Figs. 7 to 10 b) further evidences that certain planes are more prone to be strained during macroscopic elastic deformation. For example, while the M (1 0 0) and M (1 0 1) peaks almost do not shift at 100 and 220 MPa (refer to Figs. 7 and 8 b), a more evident peak shift is observed for the H (0 2 10), H (0 4 0) and M (0 2 0) planes (refer to Figs. 9 and 10 b). Furthermore, the azimuthal dependence with macroscopic deformation is also seen to be plane-dependent as evidence for the M (-1 1 1), which presents the highest relative variation (along multiple consecutive azimuthal angles) as detailed in Fig. 8 b).

Conclusions

The micromechanical elastic behaviour of a NiTiHf high temperature shape memory alloy obtained by laser powder bed fusion was evaluated using synchrotron radiation for the first time. At room temperature and after a two-step heat treatment, the material showed a dual phase microstructure composed by martensite and H-phase. During macroscopic elastic loading an anisotropic deformation behaviour was observed for all analysed planes, although the (-1 0 1) martensite plane presented the lowest anisotropy.

This work also evidences for the first time the micromechanical behaviour of H-phase in high temperature shape memory alloys. It is observed that H-phase is highly compliant, at least for the analysed planes considered.

Future work will focus on the deformation mechanisms during macroscopic plastic deformation of these laser powder bed fusion alloys.

Declaration of Competing Interests

The authors declare that they have no known competing financial interests or personal relationships that could have appeared to influence the work reported in this paper.

Acknowledgements

JPO and JS acknowledge Fundação para a Ciência e a Tecnologia (FCT - MCTES) for its financial support via the project UID/00667/2020 (UNIDEMI). JS acknowledges the China Scholarship Council for funding the Ph.D. grant (CSC NO. 201808320394). ZZ acknowledges Science and Technology Project of Sichuan Province (2020ZDZX0015). The authors acknowledge DESY (Hamburg, Germany), a member of the Helmholtz

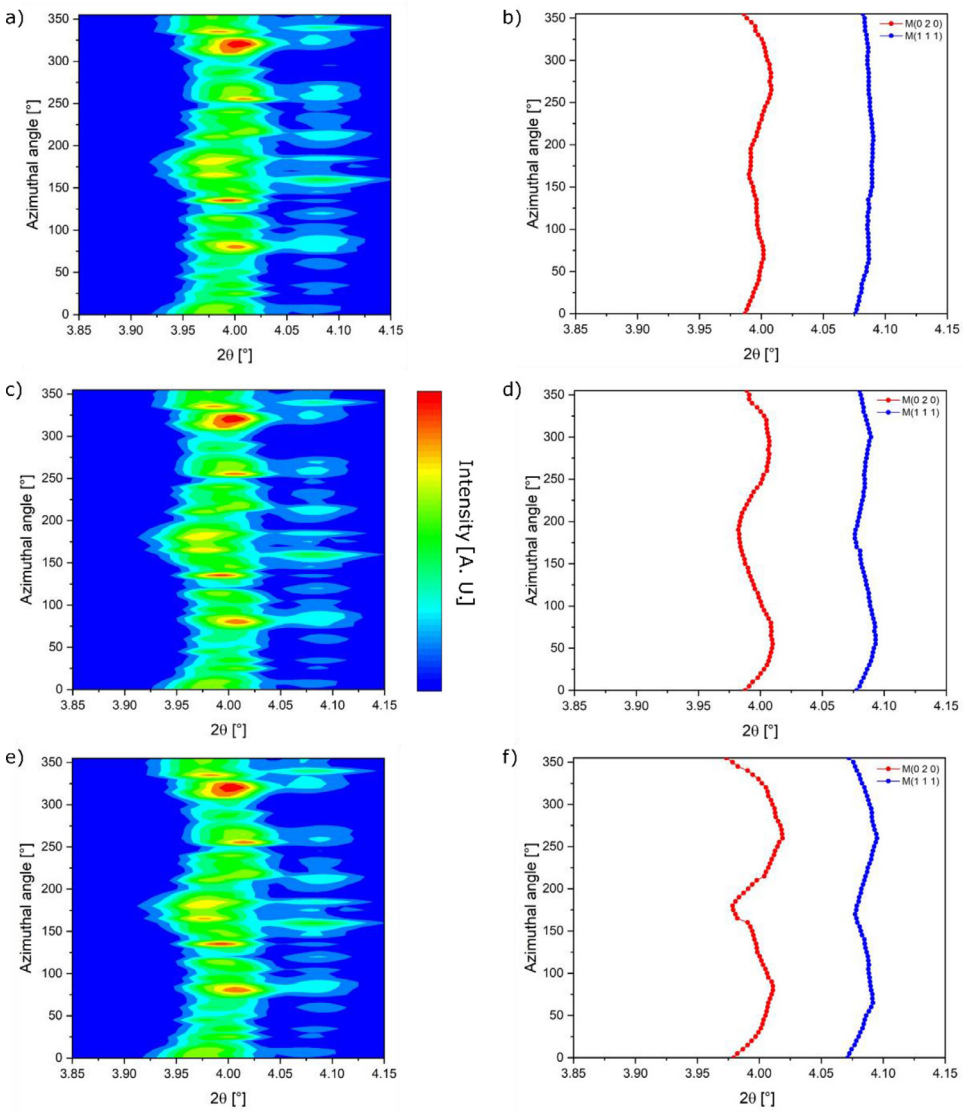

Fig. 10. Contour plot detailing the evolution of the diffracted intensity of martensite peaks M (0 2 0) and M (1 1 1) as a function of the azimuthal and diffraction angle under different loading conditions: a) before loading; b) 100 MPa; c) 200 MPa.

Association HGF, for the provision of experimental facilities. Beamtime was allocated for proposal I-20200633 EC. The research leading to this result has been supported by the project CALIPSOplus under the Grant Agreement 730872 from the EU Framework Programme for Research and Innovation HORIZON 2020.

References

[1] J.P. Oliveira, R.M. Miranda, F.M. Braz Fernandes, Welding and joining of NiTi shape memory alloys: a review, Prog. Mater. Sci. 88 (2017) 412–466, doi:10.1016/j.pmatsci.2017.04.008.

[2] M. Elahinia, N. Shayesteh Moghaddam, M. Taheri Andani, A. Amerinatanzi, B.A. Bimber, R.F. Hamilton, Fabrication of NiTi through additive manufacturing: a review, Prog. Mater. Sci. 83 (2016) 630–663, doi:10.1016/j.pmatsci.2016.08.001.

[3] R.F. Hamilton, B.A. Bimber, M. Taheri Andani, M. Elahinia, Multi-scale shape memory effect recovery in NiTi alloys additive manufactured by selective laser melting and laser directed energy deposition, J. Mater. Process. Technol. 250 (2017) 55–64, doi:10.1016/j.jmatprotec.2017.06.027.

[4] J. Ma, B. Franco, G. Tapia, K. Karayagiz, L. Johnson, J. Liu, R. Arroyave, I. Karaman, A. Elwany, Spatial Control of Functional Response in 4D-Printed Active Metallic Structures, Sci. Rep. 7 (2017) 46707, doi:10.1038/srep46707.

[5] S. Saedi, A.S. Turabi, M.T. Andani, N.S. Moghaddam, M. Elahinia, H.E. Karaca, Texture, aging, and superelasticity of selective laser melting fabricated Ni-rich NiTi alloys, Mater. Sci. Eng. A. 686 (2017) 1–10, doi:10.1016/j.msea.2017.01.008.

[6] M. Elahinia, N. Shayesteh Moghaddam, A. Amerinatanzi, S. Saedi, G.P. Toker, H. Karaca, G.S. Bigelow, O. Benafan, Additive manufacturing of NiTiHf high temperature shape memory alloy, Scr. Mater. 145 (2018) 90–94, doi:10.1016/j.scriptamat.2017.10.016.

[7] O. Benafan, M.R. Moholt, M. Bass, J.H. Mabe, D.E. Nicholson, F.T. Calkins, Recent Advancements in Rotary Shape Memory Alloy Actuators for Aeronautics, Shape Mem. Superelasticity 5 (2019) 415–428, doi:10.1007/s40830-019-00260-3.

[8] A. Evirgen, J. Pons, I. Karaman, R. Santamarta, R.D. Noebe, H-Phase Precipitation and Martensitic Transformation in Ni-rich Ni–Ti–Hf and Ni–Ti-Zr High-Temperature Shape Memory Alloys, Shape Mem. Superelasticity. 4 (2018) 85–92, doi:10.1007/s40830-018-0165-0.

[9] S.M. Kornegay, M. Kapoor, B. Chad Hornbuckle, D. Tweddle, M.L. Weaver, O. Benafan, G.S. Bigelow, R.D. Noebe, G.B. Thompson, Influence of H-phase precipitation on the microstructure and functional and mechanical properties in a Ni-rich NiTiZr shape memory alloy, Mater. Sci. Eng. A. 801 (2021) 140401, doi:10.1016/j.msea.2020.140401.

[10] S. Liu, B.B. Kappes, B. Amin-ahmadi, O. Benafan, X. Zhang, A.P. Stebner, Physics-informed machine learning for composition – process – property design: Shape memory alloy demonstration, Appl. Mater. Today. 22 (2021) 100898, doi:10.1016/j.apmt.2020.100898.

[11] S.H. Mills, C. Dellacorte, R.D. Noebe, B. Amin-Ahmadi, A.P. Stebner, Rolling contact fatigue deformation mechanisms of nickel-rich nickel-titanium-hafnium alloys, Acta Mater 209 (2021) 116784, doi:10.1016/j.actamat.2021.116784.

[12] O. Benafan, R.D. Noebe, S.A. Padula, R. Vaidyanathan, Microstructural response during isothermal and isobaric loading of a precipitation-strengthened Ni-29.7Ti-20Hf high-temperature shape memory alloy, Metall. Mater. Trans. A Phys. Metall. Mater. Sci. 43 (2012) 4539–4552, doi:10.1007/s11661-012-1297-z.

[13] O. Benafan, A. Garg, R.D. Noebe, G.S. Bigelow, S.A. Padula, D.J. Gaydosh, N. Schell, J.H. Mabe, R. Vaidyanathan, Mechanical and functional behavior of a Ni-rich Ni50.3Ti 29.7Hf20 high temperature shape memory alloy, Intermetallics 50 (2014) 94–107, doi:10.1016/j.intermet.2014.02.006.

[14] A. Shuitcev, R.N. Vasin, X.M. Fan, M.M. Balagurov, I.A. Bobrikov, L. Li, I.S. Golovin, Y.X. Tong, Volume effect upon martensitic transformation in Ti29.7Ni50.3Hf20 high temperature shape memory alloy, Scr. Mater. 178 (2020) 67–70, doi:10.1016/j.scriptamat.2019.11.004.

[15] A. Shuitcev, R.N. Vasin, M. Balagurov, L. Li, I.A. Bobrikov, Y.X. Tong, Thermal expansion of martensite in Ti29.7Ni50.3Hf20 shape memory alloy, Intermetallics 125 (2020) 18–20, doi:10.1016/j.intermet.2020.106889.

[16] A.P. Stebner, S.C. Vogel, R.D. Noebe, T.A. Sisneros, B. Clausen, D.W. Brown, A. Garg, L.C. Brinson, Micromechanical quantification of elastic, twinning, and slip strain partitioning exhibited by polycrystalline, monoclinic nickel–titanium during large uniaxial deformations measured via in-situ neutron diffraction, J. Mech. Phys. Solids. 61 (2013) 2302–2330, doi:10.1016/j.jmps.2013.05.008.

[17] J.P. Oliveira, J. Shen, J.D. Escobar, C.A.F. Salvador, N. Schell, N. Zhou, O. Benafan, Laser welding of H-phase strengthened Ni-rich NiTi-20Zr high temperature shape memory alloy, Mater. Des. 202 (2021) 109533, doi:10.1016/j.matdes.2021.109533.

[18] J.P. Oliveira, N. Schell, N. Zhou, L. Wood, O. Benafan, Laser welding of precipitation strengthened Ni-rich NiTiHf high temperature shape memory alloys: Microstructure and mechanical properties, Mater. Des. 162 (2019) 229–234, doi:10.1016/j.matdes.2018.11.053.

[19] A.P. Hammersley, S.O. Svensson, M. Hanfland, A.N. Fitch, D. Hausermann, Two-dimensional detector software: From real detector to idealised image or two-theta scan, High Press. Res 14 (1996) 235–248, doi:10.1080/08957959608201408.

[20] J.P. Oliveira, F.M. Braz Fernandes, R.M. Miranda, N. Schell, J.L. Ocaña, Effect of laser welding parameters on the austenite and martensite phase fractions of NiTi, Mater. Charact. 119 (2016) 148–151, doi:10.1016/j.matchar.2016.08.001.

[21] B.H. Toby, R.B. Von Dreele, GSAS-II : the genesis of a modern open-source all purpose crystallography software package, J. Appl. Crystallogr. 46 (2013) 544–549, doi:10.1107/S0021889813003531.

[22] L. Lutterotti, R. Vasin, H.-R. Wenk, Rietveld texture analysis from synchrotron diffraction images. I. Calibration and basic analysis, Powder Diffr 29 (2014) 76–84, doi:10.1017/S0885715613001346.

[23] M. Nematollahi, G.P. Toker, K. Safaei, A. Hinojos, S.E. Saghaian, O. Benafan, M.J. Mills, H. Karaca, M. Elahinia, Laser Powder Bed Fusion of NiTiHf High-Temperature Shape Memory Alloy: Effect of Process Parameters on the Thermomechanical Behavior, Metals (Basel) 10 (2020) 1522, doi:10.3390/met10111522.

[24] J. Zhang, S. Hao, D. Jiang, Y. Huan, L. Cui, Y. Liu, H. Yang, Y. Ren, In situ synchrotron high-energy X-ray diffraction study of microscopic deformation behavior of a hard-soft dual phase composite containing phase transforming matrix, Acta Mater 130 (2017) 297–309, doi:10.1016/j.actamat.2017.03.052.

[25] K. Otsuka, X. Ren, Physical metallurgy of Ti-Ni-based shape memory alloys, Prog. Mater. Sci. 50 (2005) 511–678, doi:10.1016/j.pmatsci.2004.10.001.

[26] B. Amin-Ahmadi, J.G. Pauza, A. Shamimi, T.W. Duerig, R.D. Noebe, A.P. Stebner, Coherency strains of H-phase precipitates and their influence on functional properties of nickel-titanium-hafnium shape memory alloys, Scr. Mater. 147 (2018) 83–87, doi:10.1016/j.scriptamat.2018.01.005.